geotechnics

MDPI

Article

Quantifying Particle Breakage and Its Evolution Using Breakage Indices and Grading Entropy Coordinates

James Leak [1], Daniel Barreto [1,*], Vasiliki Dimitriadi [1] and Emőke Imre [2]

[1] School of Computing, Engineering and the Built Environmet, Merchiston Campus, Edinburgh Napier University, Edinburgh EH10 5DT, UK
[2] Bánki Donát Faculty of Mechanical and Safety Engineering, EKIK Hydro-Bio-Mechanical Systems Research Center, Óbuda University, 1037 Budapest, Hungary
* Correspondence: d.barreto@napier.ac.uk

Abstract: Particle breakage in soils is a well-recognised behaviour. Conventional methods for quantifying the breakage process rely on calculating the area between the particle size distribution (PSD) curves produced before and after crushing. A key aspect of breakage is understanding the process across the different size/sieve fractions. Grading entropy coordinates allow for the representation of any PSD to be shown as a single point on a Cartesian plane and are able to track grading evolution with relative ease. In this study, grading entropy coordinates are compared to three commonly used breakage indices (B_r, B_r* and I_G). It is shown that grading entropy coordinates are advantageous over the traditional indices in quantifying subtle changes in the PSD evolution and directly provide further insight with regards to the individual fraction sizes. It is also discussed that conventional breakage indices rely on relative measures and are dependent on assumptions of an initial and/or final PSD. In contrast, grading entropy coordinates depend only on the characteristics of the (current) PSD curve. It was also observed that the breakage evolution captured by the entropy coordinates is able to determine the rate at which differently sized particles break as differently sized particles take on stress. Moreover, it is suggested that entropy coordinates may also stress path dependency, a feature not present in conventional indices.

Keywords: particle breakage; grading entropy; grading entropy coordinates; PSD; breakage indices

Citation: Leak, J.; Barreto, D.; Dimitriadi, V.; Imre, E. Quantifying Particle Breakage and Its Evolution Using Breakage Indices and Grading Entropy Coordinates. *Geotechnics* **2022**, 2, 1109–1126. https://doi.org/10.3390/geotechnics2040052

Academic Editor: Fatin N. Altuhafi

Received: 1 November 2022
Accepted: 2 December 2022
Published: 10 December 2022

1. Introduction

Particle breakage in soils is a well-recognised behaviour and has been widely investigated. It is influenced by both chemical composition and mechanical processes [1–5]. Many have proposed methods for quantifying the breakage process and several of these methods rely on quantifying the area between the particle size distribution (PSD) curves produced before and after crushing, e.g., [6–8].

Geomechanical research has provided significant insight into particle breakage behaviour. Various studies have proposed physically-based particle breakage criteria for DEM simulations of single particle crushing, e.g., [9]. The evolution of particle contacts during shear whilst accounting for particle breakage has been extensively studied [10–12]. Experimentally, X-ray tomography in conjunction with image analysis has been used to further understand microstructural processes during particle breakage and emphasised the effects of particle morphology on particle breakage mechanisms [3]. Experimental and numerical data has also suggested that large particles break first, followed by smaller particles as stresses are redistributed via changes in the force chains structure e.g., [6,13–17]. The grading state index I_G, from [17], has been used in DEM simulations to produce a relationship between breakage evolution and the shifting of the critical state line (CSL), concluding that breakage evolution is important in the description of the critical state of soils [11].

As evidenced by the previous studies, the quantification of particle breakage is necessary. It has been observed that it affects soil stiffness, volumetric response, and it may alter the inclination and position of the critical state line, e.g., [17,18]. As a result, different grading indices have been proposed, and with relative success, that may be included in some constitutive models [19–25]. With regards to breakage indices, early work has explicitly stated that:

> "*The problem is to choose a measure that adequately integrates the breakage occurring in the various size fractions of the material*" [6]

Whilst evaluating changes in the fraction sizes on the basis of commonly used grading indices is possible, it is not explicit. In this study, grading entropy coordinates are used as a means to quantify particle breakage to explicitly analyse changes in PSD as a result of particle breakage. Data from three different experimental data sets on different granular materials are studied here in detail. Three breakage indices developed by [6,13,17] are compared against grading entropy coordinates. It is argued that grading entropy coordinates provide an explicit evaluation of changes regarding individual size fractions and provide further insight into the evolution of particle breakage. A discussion of assumptions used in these breakage indices is also used to highlight the relativistic nature of these methods, as opposed to the entropy coordinates which are absolute.

Whilst the use of grading entropy coordinates to assess particle breakage is not new e.g., [26,27], the novelty of this work includes: (i) the comparison of the entropy coordinates to three well known breakage indices; (ii) demonstrating that grading entropy coordinates provide explicit information related to the changes in individual size fractions resulting from particle breakage, and (iii) exploring, for the first time, that grading entropy coordinates are able to capture particle breakages dependence on stress level and stress path. These three innovations imply that grading entropy can be used as a more effective means of quantifying particle breakage in granular materials than currently used methods. Using a grading entropy coordinate reduces the number of assumptions in constitutive modelling applications where breakage has to be considered. Furthermore, the use of grading entropy coordinates also enables direct and simple integration of the breakage occurring in all the various size fractions.

2. Breakage Indices

Breakage is typically characterised using various breakage indices e.g., [4,7,8,16]. A detailed overview of the many different breakage indices is presented by [28] breakage (B_t) and the breakage potential (B_p), as seen in Equation (1). The breakage potential is equal to the area between the line defining the upper limit of the silt size (d = 0.074 mm), and the part of the PSD for which d > 0.074 mm. Its value is quantified by obtaining the area between the upper and lower limits of the initial grading curve (Figure 1a). If the soil in Figure 1a is subject to crushing, the position and shape of the PSD will change. Hence, the total breakage is obtained by calculating the area between the initial and final grading curves, as seen in Figure 1b.

$$B_r = \frac{B_t}{B_p} \tag{1}$$

The definition of B_r requires two references state: the initial PSD and a limiting PSD (assuming that the soil will crush until all particles have a size d = 0.074 mm). Note that B_r = 0 indicates that no breakage has taken place, and B_r = 1 means a uniform PSD with d = 0.074 mm after breakage.

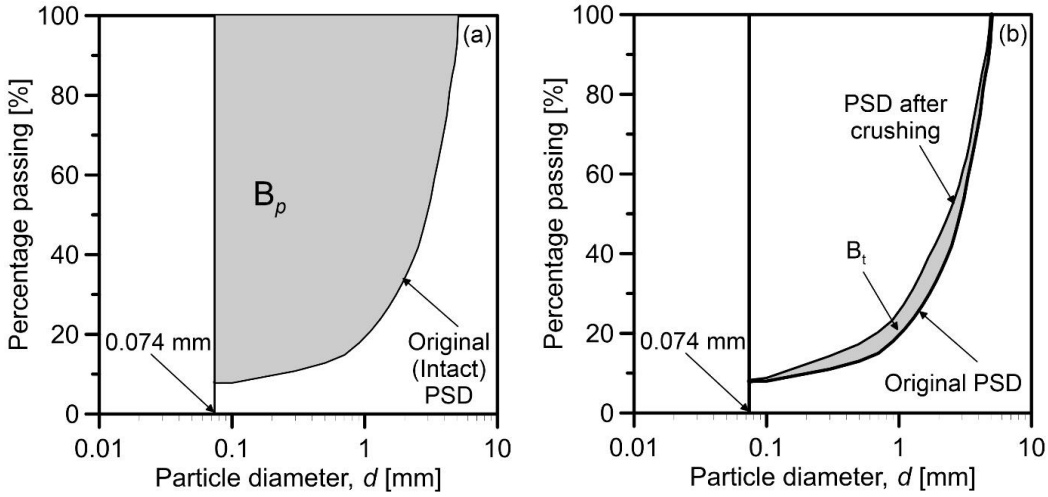

Figure 1. (**a**) Breakage potential (B_p), (**b**) Total breakage (B_t) modified after [6].

The concept of a limiting PSD has been expanded upon to incorporate fractal theory [29]. The inclusion of fractal theory means that, under loading and as a result of particle breakage, a PSD will tend towards an ultimate state with a better particle-packing efficiency. This suggests that breakage will cease to occur as the voids become increasingly filled with smaller particles [16]. A modified version of Hardin's breakage parameter (B_r) incorporates this theory, e.g., [13,14]. Here, the breakage potential (B_p) is adjusted so the final PSD is a fractal distribution, as illustrated in Figure 2. The modified relative breakage parameter (B_r*) is given by:

$$B_r^* = \frac{B_t}{B_p^*} \tag{2}$$

where B_p^* is the breakage potential (similar to Hardin's B_p) but using an assumed final fractal distribution instead of the straight line defined by Hardin's limiting size (i.e., 0.074 mm). The modified B_p* parameter is convenient, as it infers a definable limit state for the ultimate PSD within the range of 0 to 1; B_r* = 0 implies that no breakage occurs, and B_r* = 1 indicates the total breakage has produced a fractal distribution.

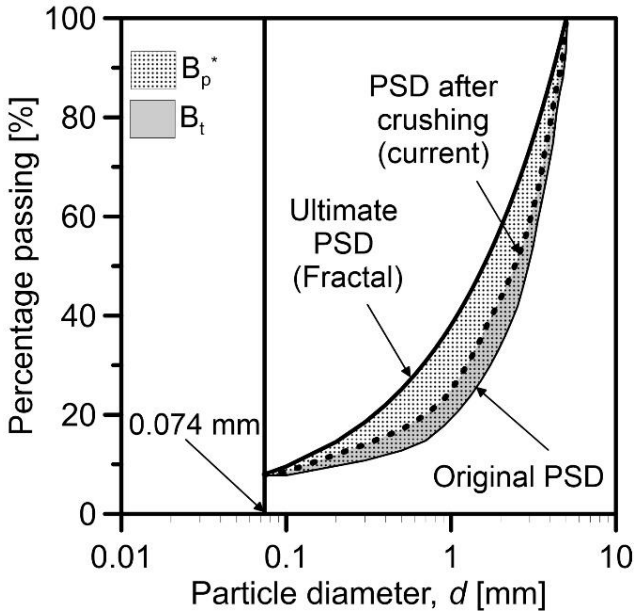

Figure 2. Modified relative breakage parameter *Br** modified after [13].

The grading state index (I_G), from [17], also modifies the relative breakage parameter (B_r^*). The grading index also accounts for an ultimate fractal distribution (see Figure 3). However, I_G seems to assume that any (initial/current) PSD is the result of previous breakage processes acting on a monodispersed PSD with $d = d_{max}$. As in the case of B_r^*, $I_G = 0$ assumes no breakage and $I_G = 1$ indicates a fractal distribution being created.

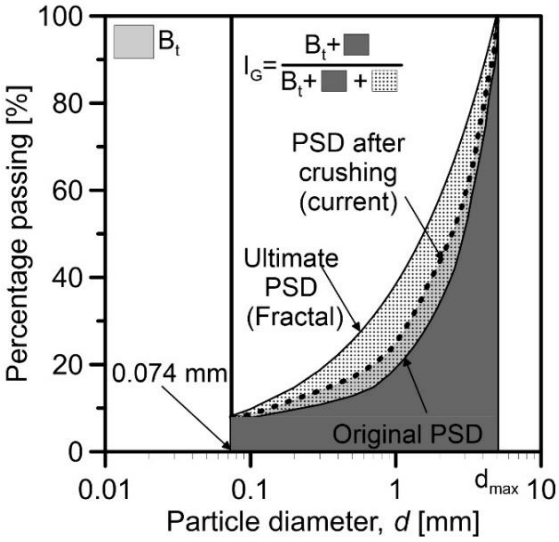

Figure 3. Determination of grading index (I_G) modified after [10].

These three breakage indices differ as a result of their assumptions on the initial and/or final distributions. In order to evaluate the differences caused by these assumptions, experimental data from [30] comprised of ring shear tests on Dog's Bay sand is used. Figure 4 shows the calculated data according to the three approaches and includes, for comparison purposes, an alternative definition that considers the breakage index to be calculated on the basis of two uniform PSDs (i.e., initial and final uniform PSDs).

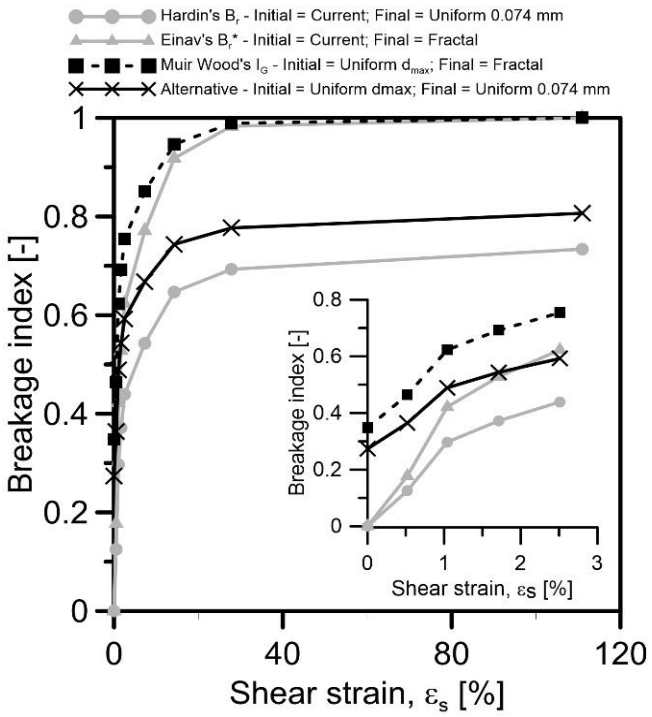

Figure 4. Breakage indices using different initial and final PSD assumptions.

In Figure 4, Hardin's B_r provides the lowest estimates, together with the alternative definition. This results from the assumption of a uniform final grading with d = 0.074 mm, which is difficult to achieve. The indices by [13,17] produce similar final results due to their common assumption of an ultimate fractal grading. However, the insert in the figure also shows that the initial points are also affected by the PSD assumptions. The B_r and B_r* indices share the same starting point, as they both assume the current grading to be the initial PSD. As can be observed for I_G, the alternative breakage index starts well above due to the initial PSD assumption. All grading indices show a rapid increase in breakage up to about 30% shear strain and only slight increases thereafter. Whilst it is now accepted that breakage progresses towards a fractal grading, a fractal grading is defined by requiring the assumption/measurement of the fractal dimension D and the maximum particle sizes, d_{max}:

$$M(\delta < d_i)/M_T = \left(\frac{d_i}{d_{max}}\right)^{(3-D)} \tag{3}$$

where $M(\delta < d_i)/M_T$ is the percentage finer than the particle diameter d_i. Independently of the assumptions, however, all the breakage indices are relative. This is a significant aspect, particularly if such indices are used as part of constitutive models and/or for the prediction of breakage quantities. In this study, the concept of grading entropy coordinates is revisited. These coordinates do not require assumptions about the initial/final grading (i.e., they are absolute, not relative) and may provide further information about the evolution of particle breakage in granular materials.

3. Grading Entropy

Proposed by [31], grading entropy draws from the definition of statistical entropy e.g., [32–34]. It allows for any PSD to be represented by a single point on a Cartesian plane. Furthermore, in contrast to other conventional approaches, it considers information pertaining to the entire PSD, rather than individual characteristic descriptors (i.e., d_{10}, d_{50}, c_u, c_c, etc.). Grading entropy coordinates have been also used to quantify other soil phenomena in addition to particle breakage [19,27], including liquefaction susceptibility [35], soil permeability [36,37], rock classification [38], and mineral dissolution effects [39,40], amongst others.

Previous work using grading entropy coordinates to analyse particle breakage in soils has focussed primarily on determining which of the entropy coordinates plays the role of the 'true' entropy, e.g., [19], observing that the entropy increment (ΔS) increases with breakage. The grading entropy approach, however, has only been compared against a limited number of existing breakage criteria, e.g., [27]. It is hoped that by doing so, it will be demonstrated that such an approach has clear advantages over traditional indices and may provide further understanding of the breakage evolution relative to the PSD fractions.

Statistical entropy (S_s) allows for the determination of the probable number of element states in a system. The concept has been applied to both the entropy of thermodynamics (S_f) and the entropy of information theory (S_i), and is given by:

$$S_s = M_s \tag{4}$$

where 'M' is the number of elements in a system, and 's' is the specific entropy given by:

$$s = -\sum_{i=1}^{m} \alpha_i log_b \alpha_i \tag{5}$$

where b is the base of the logarithm and α_i is the frequency in the i-th cell:

$$\alpha_i = \frac{M_i}{M} \tag{6}$$

The base logarithm (b) has been chosen so that it adheres to the simplest case of two cells [31], ensuring that the maximum entropy is equal to 1. Therefore, when b = 2, the specific entropy can be defined by:

$$s = -\frac{1}{\ln(2)} \sum_{i=1}^{m} \alpha_i ln\ \alpha_i \tag{7}$$

For the calculation of the grading entropy coordinates, the sieve mesh diameters increase by a magnitude of 2 (e.g., 0.25, 0.5, 1, 2, 4, 8 mm, see Table 1). Note however that this does not preclude the use of modern methods to quantify particle size (e.g., X-ray diffraction). The fractions are numbered by increasing integers, as seen in Table 1, where 'd' is the mesh diameter and S_{0i} is the Eigen-entropy of the i-th fraction (i.e., the eigen-entropies can be considered as simple integer sieve identifiers).

Table 1. Size fractions, diameter ranges and eigen-entropies.

Fraction (*i*)	**0**	...	**22**	**23**	**24**
d (mm)	2^{-22}–2^{-21}	...	1–2	2–4	4–8
S_{0i}	0	...	22	23	24

For the purpose of grading entropy, the minimum grain diameter (d_{min}) has been selected as the theoretical minimum grain size: the height of the SiO_4 tetrahedron, i.e., 2^{-22} mm [41]. A benchmarking exercise was performed by [42] to demonstrate the method's reliability.

Through inserting the relative frequencies (x_i) into Equation (7), the specific entropy is used to determine the grading entropy and can be split into two components:

$$S = \Delta S + S_0 \tag{8}$$

where S is the grading entropy, ΔS is the entropy increment, and S_0 is the base entropy. The entropy increment ΔS is defined as:

$$\Delta S = -\frac{1}{\ln(2)} \sum_{i=1}^{n} x_i ln\ x_i \tag{9}$$

where x_i is the relative frequency of the i-th fraction:

$$\sum_{i=i_1}^{i_N} x_i = 1, \quad x_i \geq 0 \tag{10}$$

N is the number of the fractions between the finest and coarsest particles. The base entropy S_0 is given by Equation:

$$S_0 = \sum_{i=1}^{n} x_i S_{0i} \tag{11}$$

These coordinates have simple physical meanings. The base entropy (S_0) is a logarithmic mean of the grain diameter which relates to the skewness of the PSD. The entropy increment (ΔS) is a measure of how much a soil is influenced by all of its fractions and relates to the kurtosis of the PSD.

Figure 5a illustrates some PSD locations in the non-normalised entropy diagram (S_0, ΔS) as relative frequency diagrams, whilst Figure 5b illustrates these with standard PSD plots. Note that on the x-axis, the base entropy directly relates to particle size (ranges as detailed in Table 1). Point A at the origin represents a uniform PSD with material retained only in the smallest sieve, whilst Point C is a uniform PSD with material retained only in the largest sieve. Points A, B, and C show that PSDs with material retained in only one sieve

have $\Delta S = 0$. Points E and F demonstrate that as material is retained in more sieves, the value of ΔS increases. Points G and H represent fractal distributions with d_{max} = 4 mm and D = 2.6 and 2.4, respectively. Figure 5c illustrates the relationship between non-normalised entropy coordinates (S_0, ΔS) and common PSD descriptors. The insert at the top of the entropy diagram shows several gradings with an equal value of d_{50} and different c_u values. Since the mean particle size (d_{50}) is the same for all of these gradings, they plot as points in a vertical line with S_0 = 12. As the range of sizes increases (and hence c_u increases), the value of ΔS also increases. Similarly, the insert to the right of Figure 5c represents PSD with equal c_u and increasing d_{50}. These gradings plot on a horizontal line of constant ΔS, and the value of S_0 increases as d_{50} increases.

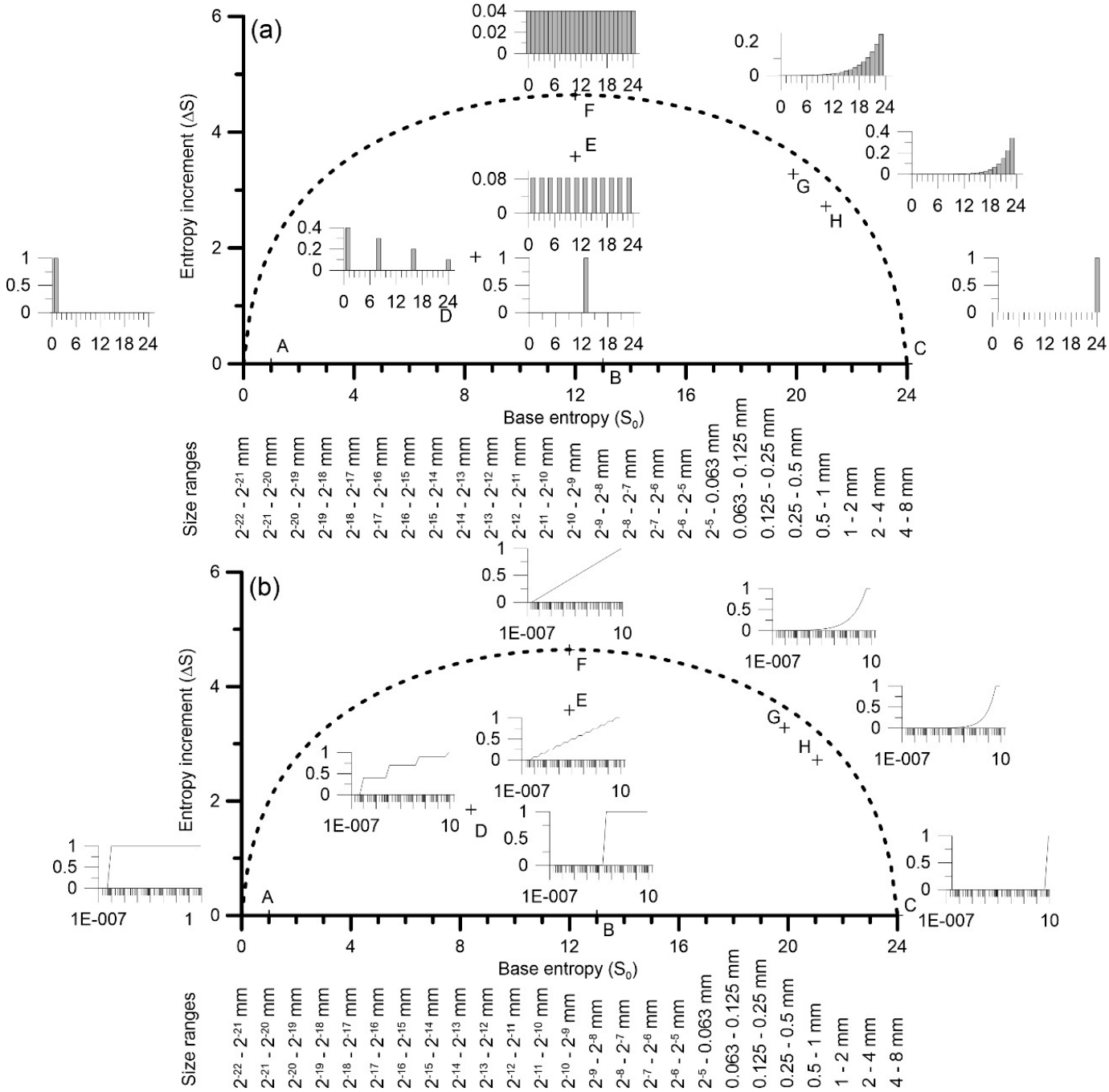

Figure 5. *Cont.*

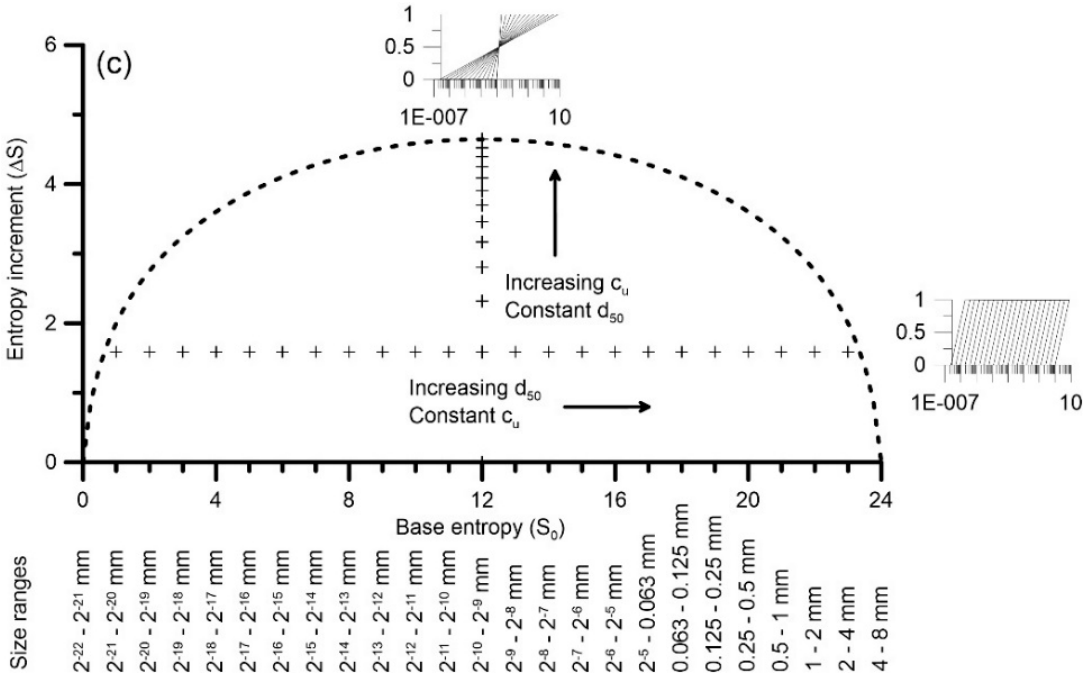

Figure 5. Non-normalised entropy diagram illustrating (**a**) relative frequency diagrams for typical PSDs, (**b**) standard grading graphs for typical PSDs, and (**c**) changes in common PSD descriptors.

Whilst grading entropy coordinates may be related to commonly used descriptors, it may be noted that in contrast to these, ΔS and S_0 involve information about the entire PSD, not just specific particle diameters (e.g., d_{10}, d_{30}, d_{60}) and enable the direct consideration of both fines and gravel content with no need for additional descriptors. Note that ΔS and S_0 may be normalised such that $0 < A < 1$ and $0 < B < B_{max} \cong 1.41$, see [19], and hence could provide means of breakage quantification between 0 and 1 as existing breakage indices. ΔS and S_0 are however absolute (not relative) and do not depend on any initial and/or final grading. Therefore, the authors restrict this paper to the use of non-normalised entropy coordinates (S_0, ΔS).

4. Evolution of Grading Indices and Grading Entropy Coordinates on the Basis of Various Experiments

Figure 6a–c show experimental crushing data from tests on granitic gravel [7]. This data was also used by [6] to illustrate the benefits of the relative breakage index (B_r) on interpreting the PSD evolution during particle breakage. For these tests, samples were subject to constant $R = \sigma'_1/\sigma'_3$ stress paths. It can be seen that, as expected, for each case the amount of breakage increases as the value of σ'_3 increases. Breakage is stress-dependent. Figure 7a–c show the evolution of B_r, B_r^* and I_G for the same data sets.

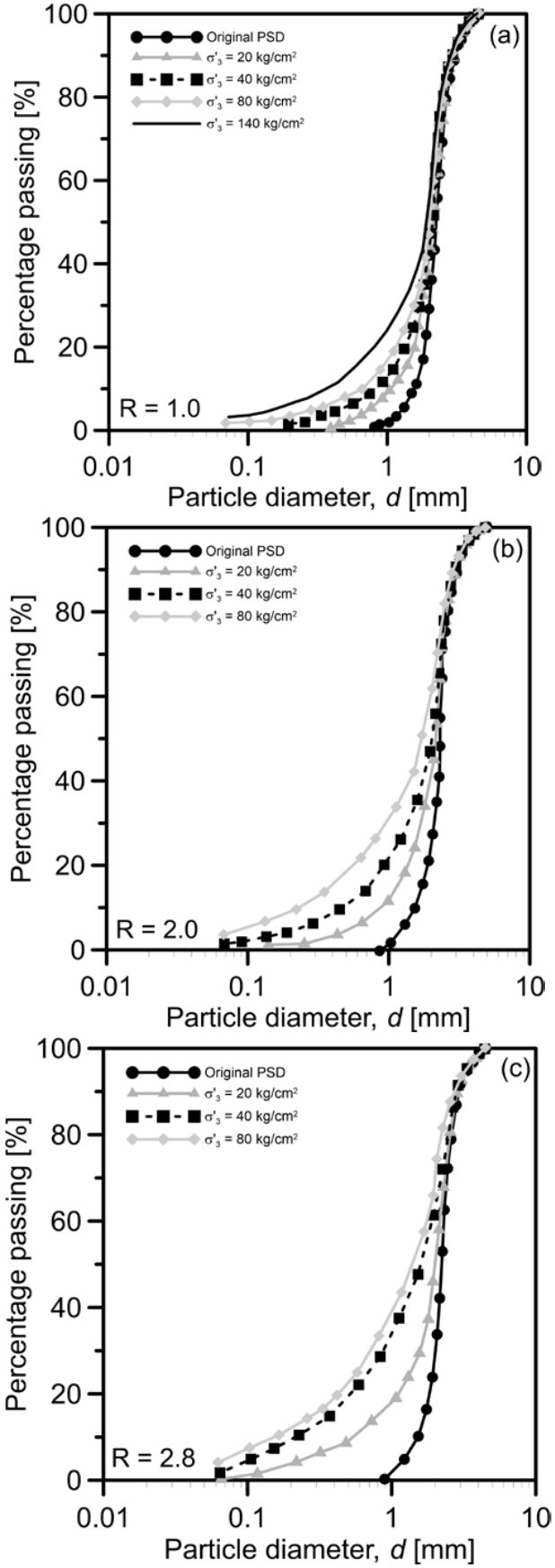

Figure 6. PSD evolution during crushing of granitic gravel at (**a**) $R = \sigma'_1/\sigma'_3 = 1.0$, (**b**) $R = \sigma'_1/\sigma'_3 = 2.0$ and (**c**) $R = \sigma'_1/\sigma'_3 = 2.8$. Modified after [7].

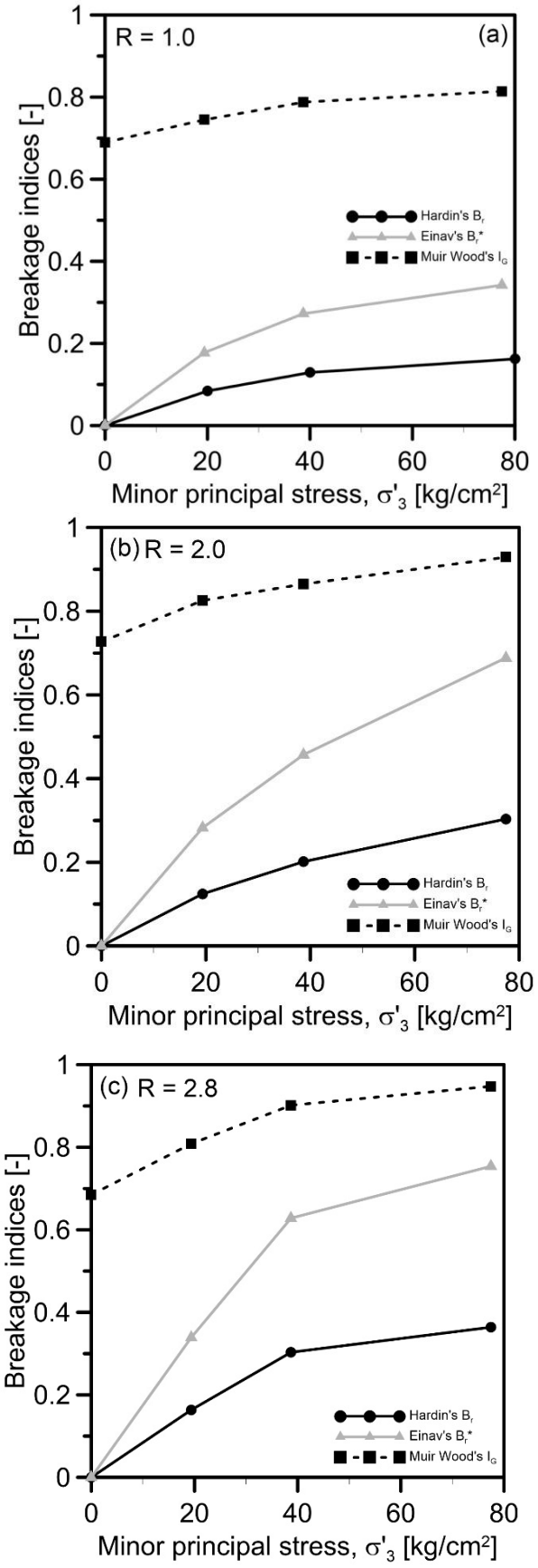

Figure 7. Evolution of B_r, B_r* and I_G during crushing of granitic gravel at (**a**) $R = \sigma'_1/\sigma'_3 = 1.0$, (**b**) $R = \sigma'_1/\sigma'_3 = 2.0$ and (**c**) $R = \sigma'_1/\sigma'_3 = 2.8$ from experimental data by [7].

The initial/final points of the curves in Figure 7 follow the same patterns discussed with reference to Figure 4. As expected, the value of all breakage indices increases as the stress level increases. In fact, there seems to be a linear increase up to 40 kg/cm^2, followed by a smaller increase thereafter. It is, however, difficult to ascertain why these changes in breakage evolution occur.

Figure 8 shows the same data set by [7], but now the PSD evolution is quantified using grading entropy coordinates. Figure 8a demonstrates that the base entropy (S_0) reduces for all R values. This is expected because the particles become smaller as crushing progresses, hence the logarithmic mean of the particle diameter has to reduce. Similarly, Figure 8b shows that for all R values, ΔS always increases. This indicates that the number of PSD fractions (i.e., number of sieves where some material is retained) is increasing as crushing progresses. The linear parts up to 40 kg/cm^2 are also detected by the entropy coordinates. Figure 8c collects data from Figure 7a–c for comparison purposes. Note that I_G, B_r and B_r* do not show a significant difference with regards to changes in R (i.e., influence of the stress path). In other words, grading entropy coordinates may be able to capture the dependence of breakage on stress level (and stress path) more clearly than other commonly used breakage indices.

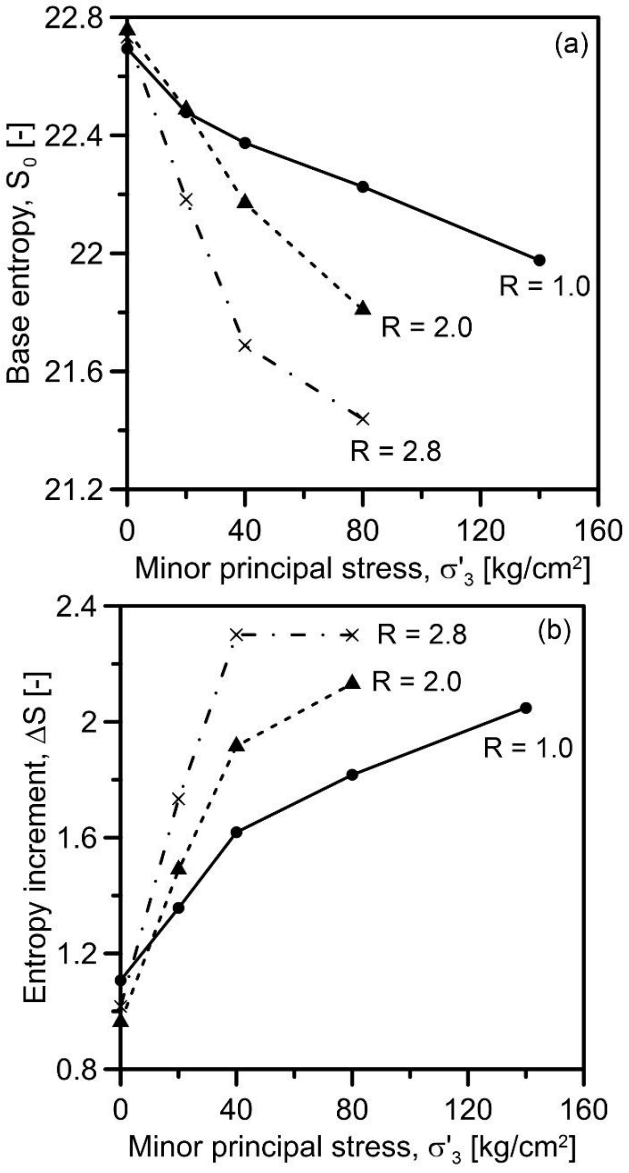

Figure 8. *Cont.*

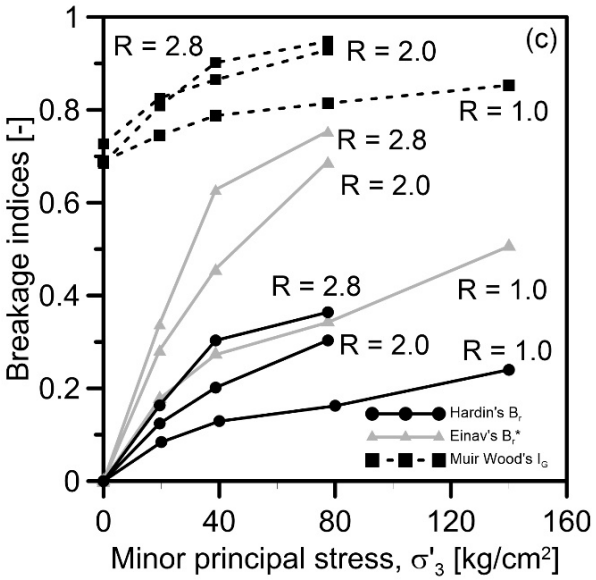

Figure 8. Evolution of grading entropy coordinates crushing of granitic gravel. (**a**) Base entropy; (**b**) entropy increment and (**c**) grading indices. All quantities calculated from experimental data by [7].

It is also now easier to interpret that the changes in gradient are the result of large particles breaking first and having a larger influence over the relative frequencies of the fractions. This aspect is discussed later in greater detail.

A series of ring shear tests on carbonate sand, from [30], have been used to measure breakage, as discussed earlier with reference to Figure 4. The PSD curves at different strain levels for these tests are shown in Figure 9. As before, the evolutions of breakage indices B_r, B_r* and I_G, and the grading entropy coordinates have been obtained for each PSD and are illustrated in Figure 10.

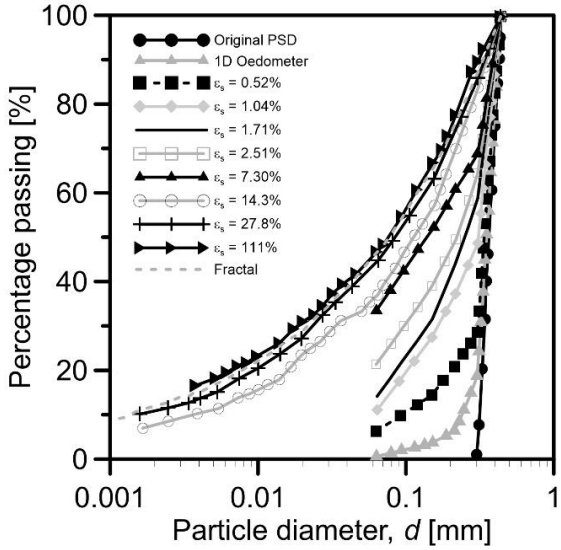

Figure 9. Evolution of PSD during ring shear tests for Dog's Bay sand. Modified after [30].

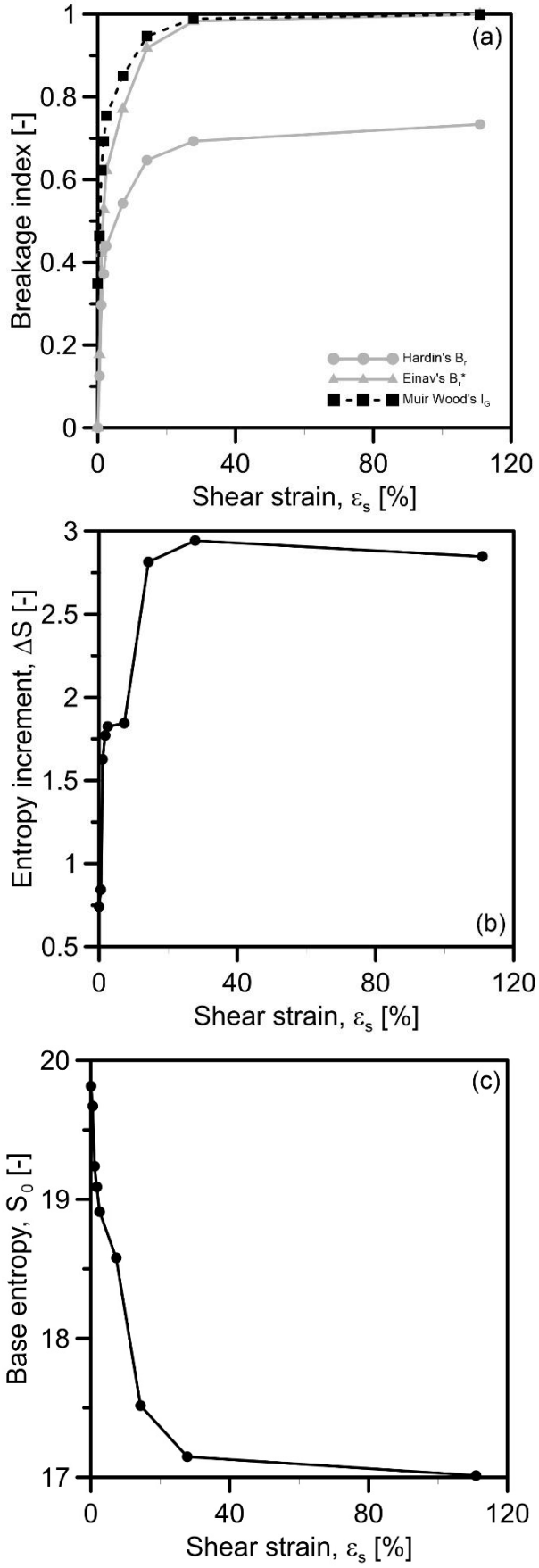

Figure 10. Evolution of (**a**) breakage indices, (**b**) base entropy and (**c**) entropy increment calculated based on experimental data on Dog's Bay sand by [30].

Referring to Figure 10a, it is clear that both B_r* and I_G approach the value of 1.0 because the final gradings are very close to a fractal distribution. The evolution of all indices is however very similar, once again with the largest changes occurring at the initial stage (i.e., $\varepsilon_a < 30\%$) of the tests. Figure 10b,c also show similar trends, as discussed before. Notably, in Figure 10b, between strains 2.51% and 7.3%, there is little change in the entropy increment. Here, the curves produced by these strain increments consist of a roughly similar number of fractions. However, observing the base entropy in Figure 10c there is a clear reduction in the mean grain diameter (because a decrease in S_0 indicates a decrease in logarithmic mean particle size). This observation is useful, as it highlights the complementary nature of the entropy coordinates. Moreover, it is important to note that whilst the breakage indices in Figure 10a are unable to produce a significant difference in value between shear strains, at 2.51% and 7.3%, the grading entropy coordinates are much more sensitive and can clearly discern between these similar, yet different, PSDs.

Using grading entropy coordinates to analyse experimental data from other researchers e.g., ref. [30], has suggested that they are able to account for stress level and stress path dependency. They have also been shown to be more sensitive than the three compared breakage indices and are able to capture slight changes in the PSD as crushing progresses. It is also argued that the physical interpretation of changes in the gradient in the curves produced by the breakage indices (and grading entropy coordinates) can be readily explained with the entropy approach. With this purpose in mind, we re-examine data for crushing tests on Fountainebleu sand, from [43].

The changes in PSD during crushing up to 100 MPa are illustrated in Figure 11a. Of particular interest in this data is the rapid change in large particle sizes after crushing at 25 MPa, as observed at the top right of Figure 11a. Figure 11b shows the non-normalised entropy diagram of the same data illustrated in Figure 11a. As crushing occurs, some particles become smaller, decreasing the mean particle size of the PSD (i.e., reducing d_{50} and S_0). As expected, the base entropy (related to mean particle size) reduces as crushing progresses. Crushing evolves from right to left in the entropy diagram as indicated. Note that the entropy increment generally increases, as seen in other data, but temporarily decreases for crushing at 25 MPa. The physical meaning of this is that the largest particles have seemingly crushed first and have a larger influence over the PSD changes for this particular grading. Crushing has temporarily reduced the number of sieves that the PSD consists of during this stress increment. However, as crushing evolves and more of the smallest particles are broken, the entropy increment continues to increase. This evolution is also explained with reference to Figure 11c. In this figure each band represents the relative frequency of a size (sieve) range. The sum of all relative frequencies at any stress level are equal to 1. The original PSD (at 0 MPa) is dominated by particles between 0.0063 and 0.5 mm that have the largest thicknesses (relative frequencies, x_i) at that point. Note that at 0 MPa there is a significant proportion of larger particles between 1 and 8 mm. However, after crushing at 25 MPa, nearly all the larger particles (>1 mm) have been broken, while the quantity of other particle sizes have slightly increased. Also note how the proportion of particles between 2^{-5} and 0.125 remains relatively constant. In other words, not all particle sizes break in the same amount, nor at the same moment. This has also been observed in DEM simulations by [17]; however, it is directly quantified here (on the basis of experimental data) for the first time. These changes may be also affected by particle shape, mineralogy, initial density, and further study on these aspects are warranted. However, most importantly, these changes may be explicitly explained by using grading entropy coordinates.

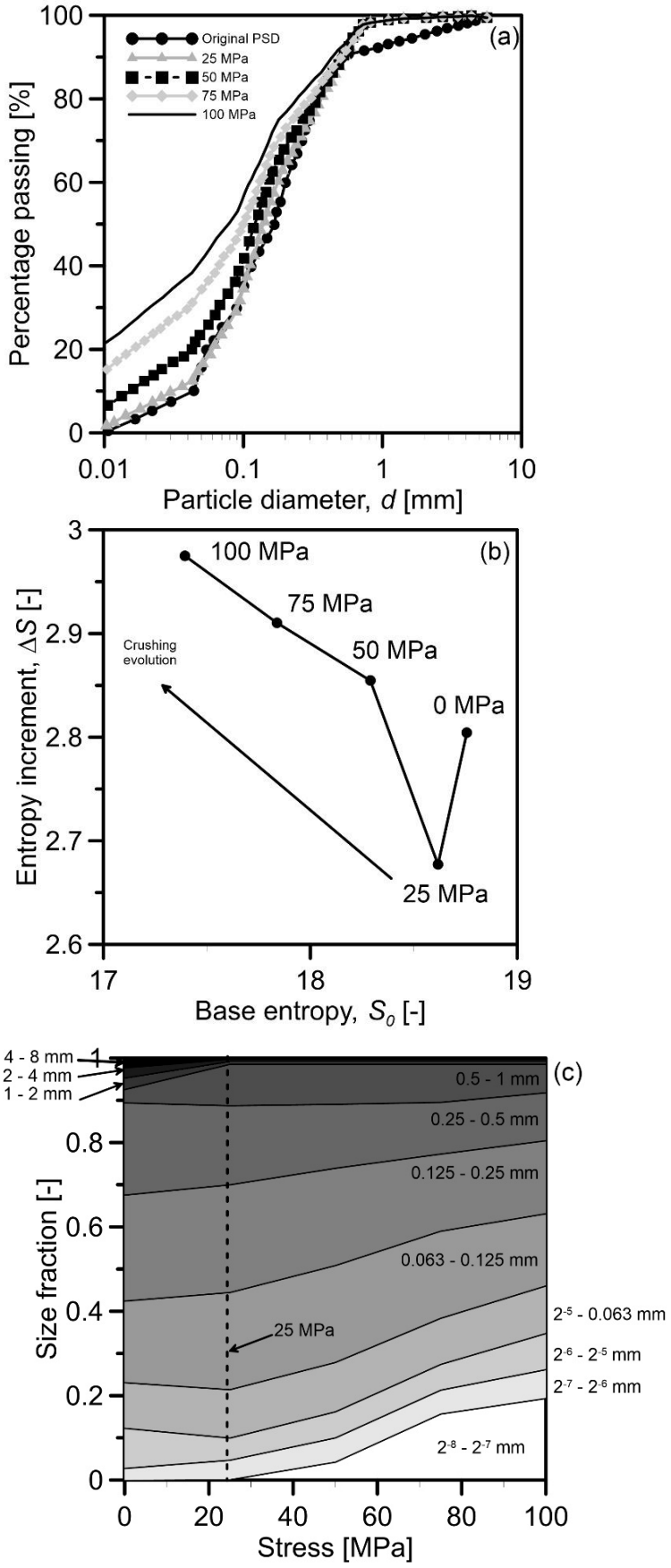

Figure 11. Evolution of (**a**) PSD curves, (**b**) grading entropy coordinates and (**c**) size fractions during crushing of Fountainbleu sand from [43].

With reference to the entropy diagram in Figure 11b, it is interesting to compare different experimental data sets within a unified context. Figure 12 shows the non-normalised entropy diagram for the three data sets discussed in this study. As expected, for all data sets, there is a reduction in base entropy (S_0) and a trend of increasing entropy increment (ΔS). Convergence of the quartz and carbonate sands towards a fractal distribution is also clear. There is also an evident difference between these sands and the gravel, which highlights the benefits of using non-relative breakage parameters. It may also be argued, as discussed by [6], that the evolution of the entropy paths may be dependent on mineralogy, as carbonate sands are more prone to breakage than quarzitic ones. This statement, however, requires further study but has also been preliminary observed by [44]

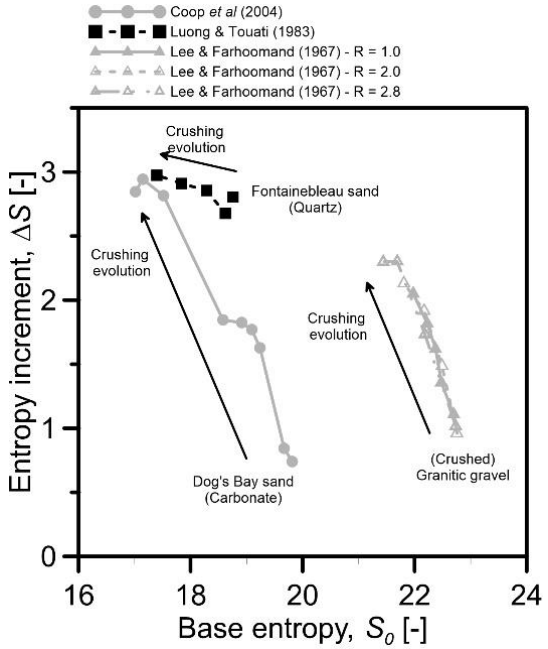

Figure 12. Evolution of grading entropy coordinates for crushed granitic gravel, quarzitic, and carbonate sands [7,30,43].

5. Discussion and Conclusions

This study has analysed the evolution of particle breakage using three breakage indices proposed by [6,13,17] and compared them to the grading entropy method proposed by [31] The three indices chosen are the most widely used ones within geotechnical engineering. The effect of breakage on stress level, stress path and material has been explored (i.e., crushed granitic gravel and quarzitic and carbonate sands). The aim of this study was to demonstrate the advantages of grading entropy coordinates to quantify breakage evolution over commonly used breakage indices. The main findings are as follows:

- Conventionally used breakage indices make use of relative measures and are therefore dependent on assumptions of an initial and/or final PSD. In contrast, non-normalised grading entropy coordinates are absolute and depend only on the characteristics of the (current) PSD. Furthermore, entropy coordinates have been seen to be highly sensitive to the way in which the particles break. This suggests that the coordinates are advantageous, as they not only relate the breakage directly to the PSD but detail the way in which different particle sizes (and materials) may break during crushing.
- Grading entropy coordinates are more sensitive to small changes in PSD, particularly for small amounts of breakage at small stresses/strains. The coordinates are suggested to be stress level- and also seemingly stress path-dependent in a more distinguishable manner. The entropy paths during breakage have a definite direction, and this may be linked to any initial PSD and may possibly enable precise predictions of PSD changes during crushing.

- Since the calculation of entropy coordinates requires direct quantification of the individual size/sieve fractions, further insights can be immediately gained. With some data analysis based on a single data set from [43], it has been demonstrated that not all the size fractions break in the same amount, nor moment (i.e., stress/strain level), aligning with the conclusions of [17].
- The change in entropy coordinates during crushing from a well-defined initial PSD can be quantified and may be used as a material characteristic. Evidence presented here shows that the change in entropy coordinates for more breakable materials is larger than that for more breakage-resistant materials.

It should be noted that this work has used only the non-normalised entropy coordinates. This decision was made to avoid issues regarding the normalisation process, which may make the PSDs size-dependant and discontinuous. Furthermore, it must be noted that grading entropy coordinates do not account for particle shape effects and their effect on soil density explicitly. As a result of these findings it is suggested that the non-normalised grading entropy coordinates may be used to gain further insight into particle breakage in soils and other granular materials. It may also be argued that such an approach may also serve as input to micro-mechanically derived constitutive relationships because the evolution of particle breakage in individual fractions can be quantified with ease and is directly linked to parameters such as initial/current density, stress level, stress path, etc.

Future investigations should emphasise an application of the entropy coordinates in existing constitutive models, to expand grading entropy applications. Moreover, the scope should be expanded to explore the breakage of a greater number of materials and also include the effects of particle shape.

Author Contributions: Conceptualization, J.L., D.B. and E.I.; methodology, J.L. and D.B. writing—original draft preparation, J.L.; writing—review and editing, D.B., E.I. and V.D.; supervision, D.B. and V.D. All authors have read and agreed to the published version of the manuscript.

Funding: This research received no external funding.

Institutional Review Board Statement: Not applicable.

Informed Consent Statement: Not applicable.

Data Availability Statement: Some or all data, models, or code that support the findings of this study are available from the corresponding author upon reasonable request.

Conflicts of Interest: The authors declare no conflict of interest.

References

1. Karatza, Z.; Andò, E.; Papanicolopulos, S.-A.; Ooi, J.Y.; Viggiani, G. Evolution of deformation and breakage in sand studied using X-ray tomography. *Géotechnique* **2018**, *68*, 107–117. [CrossRef]
2. de Bono, J.P.; McDowell, G.R. On the packing and crushing of granular materials. *Géotechnique* **2018**, *68*, 575–589. [CrossRef]
3. Kwag, J.M. Yielding stress characteristics of carbonate sand in relation to individual particle fragmentation strength. In Proceedings of the International Conference on Engineering for Calcareous Sediment, Bahrain, 21–24 February 1999; pp. 79–86.
4. McDowell, G.R.; Bolton, M.D.; Robertson, D. The fractal crushing of granular materials. *J. Mech. Phys. Solids* **1996**, *44*, 2079–2102. [CrossRef]
5. Nakata, Y.; Hyodo, M.; Hyde, A.F.L.; Kato, Y.; Murata, H. Microscopic particle crushing of sand subjected to high pressure one-dimensional compression. *Soils Found.* **2001**, *41*, 69–82. [CrossRef]
6. Hardin, B.O. Crushing of soil particles. *J. Geotech. Eng.* **1985**, *111*, 1177–1192. [CrossRef]
7. Lee, K.L.; Farhoomand, I. Compressibility and crushing of granular soil in anisotropic triaxial compression. *Can. Geotech. J.* **1967**, *4*, 68–86. [CrossRef]
8. Marsal, R.J. Large scale testing of rockfill materials. *J. Soil Mech. Found. Div.* **1967**, *94*, 27–43. [CrossRef]
9. de Bono, J.; McDowell, G. Particle breakage criteria in discrete-element modelling. *Géotechnique* **2016**, *66*, 1014–1027. [CrossRef]
10. Ciantia; Arroyo, M.; O'Sullivan, C.; Gens, A. Micromechanical inspection of incremental behaviour of crushable soils. *Acta Geotech.* **2019**, *14*, 1337–1356. [CrossRef]
11. Ciantia, M.O.; Arroyo, M.; O'Sullivan, C.; Gens, A.; Liu, T. Grading evolution and critical state in a discrete numerical model of Fontainebleau sand. *Geotechnique* **2019**, *69*, 1–15. [CrossRef]

12. Zhu, H.; Zhou, W.H.; Jing, X.Y.; Yin, Z.Y. Observations on fabric evolution to a common micromechanical state at the soil-structure interface. *Int. J. Number Anal. Methods Geomech.* **2019**, *43*, 2449–2470. [CrossRef]
13. Einav, I. Breakage mechanics-part I: Theory. *J. Mech. Phys. Solids* **2007**, *55*, 1274–1297. [CrossRef]
14. Einav, I. Breakage mechanics-part II: Modeling granular materials. *J. Mech. Phys. Solids* **2007**, *55*, 1298–1320. [CrossRef]
15. Coop, M.R.; Lee, I.K. The behaviour of granular soils at elevated stresses. In *Predictive Soil Mechanics*; Thomas Telford: London, UK, 1993.
16. McDowell, G.R.; Bolton, M.D. On the micromechanics of crushable aggregates. *Geotechnique* **1998**, *48*, 667–679. [CrossRef]
17. Muir Wood, D.; Maeda, K. Changing grading of soil: Effect on critical states. *Acta Geotech.* **2008**, *3*, 3–14. [CrossRef]
18. Ghafghazi, M.; Shuttle, D.A.; DeJong, J.T. Particle breakage and the critical state of sand. *Soils Found.* **2014**, *54*, 451–461. [CrossRef]
19. Tong, C. Particle Breakage of Granular Soils: Evolution Laws and Constitutive Modelling. Ph.D. Thesis, University of Technology Sydney, Otimo, Australia, 2020.
20. Kikumoto, M.; Wood, D.M.; Russell, A. Particle crushing and deformation behaviour. *Soils Found.* **2010**, *50*, 547–563. [CrossRef]
21. McDowell, G.R. On the yielding and plastic compression of sand. *Soils Found.* **2002**, *42*, 139–145. [CrossRef]
22. Rubin, M.B.; Einav, I. A large deformation breakage model of granular materials including porosity and inelastic distortional deformation rate. *Int. J. Eng. Sci.* **2011**, *49*, 1151–1169. [CrossRef]
23. Ueng, T.S.; Chen, T.J. Energy aspects of particle breakage in drained shear of sands. *Geotechnique* **2000**, *50*, 65–72. [CrossRef]
24. Xiao, Y.; Liu, H. Elastoplastic constitutive model for rockfill materials considering particle breakage. *Int. J. Geomech.* **2017**, *17*, 4016041. [CrossRef]
25. Yao, Y.P.; Yamamoto, H.; Wang, N.D. Constitutive model considering sand crushing. *Soils Found.* **2008**, *48*, 603–608. [CrossRef]
26. Lőrincz, J.; Imre, E.; Gálos, M.; Trang, Q.P.; Rajkai, K.; Fityus, S.; Telekes, G. Grading Entropy Variation Due to Soil Crushing. *Int. J. Geomech.* **2005**, *5*, 311–319. [CrossRef]
27. Leak, J.; Barreto, D.; Dimitriadi, V.; Imre, E. Revisiting Hardin's parameters for the quantification of particle breakage—A statistical entropy approach. *Eur. Phys. J. Conf.* **2021**, *249*, 7001. [CrossRef]
28. Yu, F. Particle breakage in granular soils: A review. *Part. Sci. Technol.* **2019**, *39*, 91–100. [CrossRef]
29. Mandelbrot, B.B. *The Fractal Geometry of Nature*; W.H. Freeman and Company: New York, NY, USA, 1983.
30. Coop, M.R.; Sorensen, K.K.; Bodas Freitas, T.; Georgoutsos, G. Particle breakage during shearing of a carbonate sand. *Geotechnique* **2004**, *54*, 157–163. [CrossRef]
31. Lőrincz, J. Grading Entropy of Soils. Ph.D. Thesis, Technical University of Budapest, Budapest, Hungary, 1986.
32. Boltzmann, L. Uber die Beziehung zwischen dem zweiten Hauptsatze der mechanischen Warmetheorie und der Wahrscheinlichkeitsrechnung respektive den Satzen uber das Warmgleichgewicht. *Weiner Ber.* **1877**, *76*, 373–435.
33. Shannon, C.E. A mathematical theory of communication. *Bell System Tech. J.* **1949**, *27*, 379–423, Reprinted in *The Mathematical Theory of Communication*; The University of Illinois Press: Urbana, IL, USA, October 1948; pp. 623–656. [CrossRef]
34. Korn, G.A.; Korn, T.M. *Matematikai Kézkönyv Mûszakiaknak; (Math. Handbook for Scientists and Engineers)*; Mûszaki Könyvkiadó: Budapest, Hungary, 1975.
35. Barreto, D.; Leak, J.; Dimitriadi, V.; McDougall, J.; Imre, E.; Lőrincz, J. Grading entropy coordinates and criteria for evaluation of liquefaction susceptibility. In *Earthquake Geotechnical Engineering for Protection and Development of Environment and Constructions*; CRC Press: Rome, Italy, 2019. [CrossRef]
36. Feng, S.; Vardanega, P.J.; Ibraim, E.; Widyatmoko, I.; Ojum, C. Permeability assessment of some granular mixtures. *Géotechnique* **2019**, *69*, 646–654. [CrossRef]
37. O'Kelly, B.C.; Nogal, M. Determination of soil permeability coefficient following an updated grading entropy method. *Geotech. Res.* **2020**, *7*, 58–70. [CrossRef]
38. Imre, E. Grading Entropy and Degradation of Sands and Rocks. In Proceedings of the 2nd International Electronic Conference on Entropy and Its Applications, Santa Barbara, CA, USA, 15–30 November 2015. [CrossRef]
39. McDougall, J.; Kelly, D.; Barreto, D. Particle loss and volume change on dissolution: Experimental results and analysis of particle size and amount effects. *Acta Geotech.* **2013**, *8*, 619–627. [CrossRef]
40. McDougall, J.R.; Imre, E.; Barreto, D.; Kelly, D. Volumetric consequences of particle loss by grading entropy. *Géotechnique* **2013**, *63*, 262–266. [CrossRef]
41. Imre, E. Characterization of dispersive and piping soils. In Proceedings of the 11th ECSMFE, Copenhagen, Denmark, 28 May–1 June 1995; Volume 2, pp. 49–55.
42. Imre, E.; Lörincz, J.; Szendefy, J.; Trang, P.Q.; Nagy, L.; Singh, V.P.; Fityus, S. Case studies and benchmark examples for the use of grading entropy in geotechnics. *Entropy* **2012**, *14*, 1079–1102. [CrossRef]
43. Luong, M.P.; Touati, A. Sols grenus sous fortescontraintes. *Rev. Française De Géotechnique* **1983**, *24*, 51–63. [CrossRef]
44. Lőrincz, J.; Imre, E.; Trang, P.Q.; Gálos, M.; Karpati, L.; Talata, I.; Barreto, D.; Casini, F.; Guida, G. New method for rock qualification. In Proceedings of the Mérnökgeológia-Kőzetmechanika, Budapest, Hungary, 19 April 2018; pp. 263–274.